

An overview of the spectral induced polarization method for near-surface applications

Andreas Kemna^{1*}, Andrew Binley², Giorgio Cassiani³, Ernst Niederleithinger⁴,
André Revil^{5,6}, Lee Slater⁷, Kenneth H. Williams⁸, Adrián Flores Orozco¹,
Franz-Hubert Haegel⁹, Andreas Hördt¹⁰, Sabine Kruschwitz⁴, Virginie Leroux¹¹,
Konstantin Titov¹², Egon Zimmermann¹³

¹Geodynamics/Geophysics, Steinmann Institute, University of Bonn, Germany

²Lancaster Environment Centre, Lancaster University, UK

³Department of Geosciences, Padova University, Italy

⁴BAM Federal Institute for Materials Research and Testing, Berlin, Germany

⁵Department of Geophysics, Colorado School of Mines, Golden, USA

⁶ISTerre, CNRS, UMR CNRS 5275, Université de Savoie, Le Bourget du Lac, France

⁷Department of Earth and Environmental Sciences, Rutgers-Newark, Newark, USA

⁸Earth Sciences Division, Lawrence Berkeley National Laboratory, Berkeley, USA

⁹Agrosphere (IBG 3), Forschungszentrum Jülich GmbH, Jülich, Germany

¹⁰Institute for Geophysics and Extraterrestrial Physics, Technical University of
Braunschweig, Germany

¹¹Department of Electrical Measurements and Automation, Lund University, Sweden

¹²Department of Geophysics, St. Petersburg State University, Russia

¹³Institute for Electronics (ZEL), Forschungszentrum Jülich GmbH, Jülich, Germany

*Corresponding author e-mail: kemna@geo.uni-bonn.de; phone +49 228 73-3060

Keywords: SIP method, Electrical, Hydrogeophysics

ABSTRACT

Over the last 15 years significant advancements in induced polarization (IP) research have taken place, particularly with respect to spectral IP (SIP), concerning the understanding of the mechanisms of the IP phenomenon, the conduction of accurate and broadband laboratory measurements, the modelling and inversion of IP data for imaging purposes, and the increasing application of the method in near-surface investigations. We here summarized the current state of the science of the SIP method for near-surface applications and describe which aspects still represent open issues and should be the focus of future research efforts. Significant progress has been made over the last decade in the understanding of the microscopic mechanisms of IP; however, integrated mechanistic models involving the different possible polarization processes at the grain/pore scale are still lacking. A prerequisite for the advances in the mechanistic understanding of IP was the development of improved laboratory instrumentation, which has led to a continuously growing database of SIP measurements on various soil and rock samples. We summarize the experience of numerous experimental studies by formulating key recommendations for reliable SIP laboratory measurements. To make use of the established theoretical and empirical relationships between SIP characteristics and target petrophysical properties at the field scale, sophisticated forward modelling and inversion algorithms are needed. Considerable progress has been made also in this field, in particular with the development of complex resistivity algorithms allowing the modelling and inversion of IP data in the frequency domain. The ultimate goal for the future are algorithms and codes for the integral inversion of 3-D, time-

lapse and multi-frequency IP data, which defines a 5-D inversion problem involving the dimensions space (for imaging), time (for monitoring) and frequency (for spectroscopy). We also offer guidelines for reliable and accurate measurements of IP spectra, which are essential for improved understanding of IP mechanisms and their links to physical, chemical and biological properties of interest. We believe that the SIP method offers potential for subsurface structure and process characterization, in particular in hydrogeophysical and biogeophysical studies.

INTRODUCTION

The induced polarization (IP) method is a well-established geophysical exploration method. About 100 years ago, Conrad Schlumberger recognized the possibility of inferring subsurface structural information from measured voltage signals associated with ‘provoked’ polarization currents in the earth. By the 1960’s and 1970’s the method had become a popular choice for exploration of porphyry and massive sulphide deposits, given the strong IP response of the associated minerals (we refer to Seigel et al., 2007, for the early history of IP). During these early stages in the development of IP, the quantitative use of the method was hindered by instrumental and computational limitations. With the advance of multi-electrode, multi-channel IP instrumentation with improved measurement accuracy, and the availability of powerful computers to solve extensive numerical problems, IP started to be developed into a quantitative exploration tool. Furthermore, the spectral nature of the IP response, i.e., its characteristic frequency dependence, was increasingly investigated. Modern SIP instruments are now available which combine the sensitivity of this spectroscopic method with respect to structural characterization with the spatial resolution of a geophysical field method

(Figure 1). Consequently, SIP has been ‘re-discovered’ during the last two decades, particularly for hydrogeological and environmental investigations (see Revil et al., 2012a), where the flow and transport properties of rocks, fluid content and fluid chemistry are of major interest. In recent years promising novel applications of SIP have arisen, such as in the emerging field of biogeophysics for characterizing and monitoring the subsurface biogeochemical state (see Atekwana and Slater, 2009).

Seventeen years ago, Ward et al. (1995) outlined recommendations for IP research following an International Workshop on IP in Mining and the Environment held in 1994 at the University of Tucson, Arizona, in memorial of the IP pioneer John S. Sumner (Sumner, 1976). Since then significant advancements have taken place in IP, particularly in SIP, concerning the understanding of the mechanisms of the IP phenomenon, the conduction of accurate and broadband laboratory measurements, the modelling and inversion of IP data for imaging purposes, and the increasing application of the method in near-surface investigations. To discuss the current state of the science of IP in near-surface geophysics, a two-day international workshop took place at the University of Bonn between September 30 and October 1, 2009. This workshop was attended by 63 IP researchers and practitioners from 14 countries.

This overview article on the state of the science of the SIP method for near-surface applications and currently open research questions represents an outcome of this meeting. It is motivated by the aforementioned revived and growing interest in the use of the method and is presented as a follow-up statement of the text by Ward et al. (1995). We note that the intention here is not to provide a comprehensive review of SIP research over the last 15 years, but to (1) summarize the main achievements regarding theory and modelling, (2) to

formulate, based on extensive experimental experiences, recommendations regarding laboratory and field work, and (3) outline our view of the main gaps and demands in the understanding of IP mechanisms as well as in data acquisition, processing, inversion and interpretation.

The first section addresses the microscopic mechanisms of IP, where we summarize present understanding of the underlying polarization processes at the pore scale, in particular involving the electrical double layer, and then highlight currently open questions. Understanding the micro-scale physical, chemical and biological mechanisms that control IP is an essential step towards improving our ability to devise fruitful applications. A prerequisite for the advances in the understanding of SIP responses was the development of improved laboratory instrumentation and experimental practice, which allowed SIP measurements with the required sensitivity on a large number of various soil and rock samples. In the second section we identify the main experimental issues and compile key recommendations for reliable SIP laboratory measurements based on experiences over the last 15 years. To make use of the established theoretical and empirical relationships between SIP characteristics and target petrophysical properties at the field scale, sophisticated forward modelling and inversion algorithms are needed. In the third section we summarize the progress in this area over the last 15 years and describe the major challenges for future algorithm development. The successful application of the SIP method in the field is constrained by the data quality that can be obtained, sometimes under apparently unfavourable conditions. In the final section we bring forward the main problems and pitfalls in SIP field measurements, which, if ignored, can easily lead to an unsuccessful application of the method. We provide guidelines on how to best deal with these measurement issues so

that the potential of the SIP method for structure and process characterization can be better exploited in field investigations.

MECHANISMS

In their recommendations for IP research, Ward et al. (1995) pointed out that models are needed which relate the electrical responses of rocks and soils to the underlying physical and chemical processes, and particularly to their specific microgeometrical and surface chemical properties. Some progress has been made since 1995, even though the ultimate goal of fully understanding (and predicting) IP responses on the basis of the system's characteristics still lies ahead.

Induced polarization is caused by the transport and (reversible) accumulation of charge carriers (ions and electrons) in micro-heterogeneous materials (e.g., rock or soil) due to an external electric field. At low frequency this process is therefore mostly not dielectric in nature. Induced polarization phenomena can be observed both in time and in frequency (SIP) domain. Many fundamental studies have been performed on polarizations occurring in porous media and in colloidal suspensions, pointing out that five main mechanisms dominate at frequencies below 1 MHz. These mechanisms are:

- (1) the Maxwell-Wagner polarization (e.g., Alvarez, 1973; Chelidze and Gueguen, 1999; Lesmes and Morgan, 2001; Chen and Or, 2006);

- (2) the polarization of the Stern layer, i.e., the inner part of the electrical double layer (EDL) at the interface between minerals and water (e.g., de Lima and Sharma, 1992; Leroy et al., 2008; Vaudelet et al., 2011; Revil, 2012);
- (3) the polarization of the diffuse layer, i.e., the outer part of the EDL (e.g., Dukhin and Shilov, 1974; de Lima and Sharma, 1992);
- (4) the membrane polarization (e.g., Marshall and Madden, 1959; Vinegar and Waxman, 1984; Titov et al., 2002); and
- (5) the electrode polarization, observed in presence of disseminated conductive minerals (e.g., Wong, 1979; Merriam, 2007), such as pyrrhotite, chalcopyrite, pyrite and graphite, and long utilized as a tool for mining exploration (see, e.g., Seigel et al., 1997). This latter mechanism is specific to the presence of electronic conductors and will not be discussed further here.

The Maxwell-Wagner polarization is an interfacial polarization due to the discontinuity of displacement currents in a multiphase system with discontinuities of the dielectric permittivity and/or electrical conductivity at the interface between the different phases. This mechanism is controlled by the tortuosity of the different phases, their volume fractions, and the conductivity and permittivity of the different phases. The Maxwell-Wagner polarization is mainly responsible for polarization phenomena at the upper end of the considered frequency spectrum (typically above 1 kHz).

The remaining mechanisms are all related to the electro-migration of different types of charge carriers: electrons and ions. While electron migration may occur when a biotic or an abiotic redox process is involved, ionic polarization usually dominates the electro-migration polarization mechanisms in natural porous media. Ionic polarization is strongly related to the

occurrence of the EDL at the pore water-solid matrix interface. Both layers of the EDL, i.e., the Stern layer and the diffusive layer, can polarize, giving rise to three distinct cases depending on the connectivity of the solid phase (Revil and Cosenza, 2010; Figure 2). We note that in the current conceptualization of the electrochemical IP mechanisms (see Revil and Florsch, 2010, and Figure 3), diffuse layer polarization and membrane polarization are closely related.

Around a grain or through a constriction of the pore space, the difference of the fractions of current carried by cations and anions is responsible for the so-called membrane polarization (e.g., Dukhin and Shilov, 1974). This difference gives rise to the formation of a neutral cloud of ions (cations and anions) on one side of the grain, or the pore constriction, and a corresponding depletion of ions on the other side, both being aligned with the externally applied electric field. These zones of higher and lower salinities around the grain, or through the constriction, are responsible for a diffusion of ions from the high-salinity to the low-salinity zone according to their mutual diffusion coefficient (for the latter see, e.g., Revil, 1999). To understand this polarization mechanism, consider the simple case of two insulating grains (e.g., made of silica) coated by an EDL and immersed in a background electrolyte (Figure 3). The electrolyte contains a dissolved salt providing both cations and anions. We also consider a pore throat sandwiched between these two grains, following the conceptualization of membrane polarization by Revil and Florsch (2010). The presence of an externally applied electric field displaces the electrical diffuse layer. In the far-field, the cations move in the direction of the electric field and the anions move in the opposite direction. Because of the pore throat, the current is mainly restricted to the EDL. If we consider that the mineral grains are negatively charged (a typical case at circumneutral pH values; see, e.g., Skold et al., 2011), the counterions of the EDL are mostly cations. Due to

the pore throat, the fractions of the total current transported by the co-ions and the counterions (the so-called Hittorf numbers) are different in the bulk electrolyte and in the EDL. As a result, there is an increase of the salinity on one side of the grain and depletion in the salt concentration on the other side. This process is controlled by the balance between local concentration gradient and electric field, which act in opposite directions. This membrane polarization mechanism has been widely described in the literature (e.g., Marshall and Madden, 1959; Vinegar and Waxman, 1984) and is in the range of the observed low-frequency polarization phenomena, as its time constant is controlled by the mobility of ions in solution and the square of the pore throat length (e.g., Titov et al., 2002).

Composite-conductivity models exist and have been developed over the past twenty years to upscale the mechanisms outlined above to the scale of a representative elementary volume of a porous rock. For instance, Leroy et al. (2008) and Leroy and Revil (2009) recently modelled, based on the earlier works of de Lima and Sharma (1992) and Lesmes and Morgan (2001), the polarization mechanisms taking place in glass beads and in clay materials by coupling a Stern layer polarization model with an electrochemical model of the electrical double layer for silica and aluminosilicates and adding the effect of the Maxwell-Wagner polarization. In their approach, heterogeneity is accounted for by using (a) the polarization model for a single grain convoluted by a function determined from the particle size distribution and (b) a differential effective medium approach for modelling the electromagnetic interactions between all the grains. This approach provides an explicit relationship between the distribution of relaxation times and the grain/pore size distribution and can be used, for instance, to provide a theoretical understanding of the empirical Cole-Cole model (see also Revil and Florsch, 2010).

While the physicochemical mechanisms of polarization are well understood for simple model cases and upscaling approaches like those mentioned above exist, the link between the observed SIP response at the lab or the field scale and these fundamental processes is not fully established. In particular, the links between IP and porous media characteristics (including micro-structure, porosity, permeability, specific internal surface, tortuosity, fluid phase distribution etc.) need to be further investigated. The recent work by Revil and Florsch (2010) represents a step in this direction, although the role of membrane polarization is still unaccounted for. It is possible that the approach pursued by Vinegar and Waxman (1984) in incorporating empirically both the Stern layer and membrane polarization together could be applied to the more mechanistic models developed recently, but a unified model remains to be developed. Only with the availability of constitutive relationships at the scale of the representative elementary volume of a porous medium we will be able to effectively apply IP beyond the stage of empiricism. Modelling approaches, such as on EDL interactions between mineral grains (e.g., Kwon et al., 1998) or on the electro-diffusive transport of ions in representative pore space geometries (e.g., Blaschek and Hördt, 2009), could improve the quantitative understanding of charge distribution in the pore space and thus the SIP response. In particular, the following challenges can be identified for the near future:

- (1) The description of all the mechanisms using a mechanistic approach, and development of a general framework in which all these mechanisms are explained and quantified in their relative importance case by case;
- (2) an assessment of linearity versus non-linearity (referring to the relationship between the IP response and the strength of the exciting electric field) for the different mechanisms;

- (3) the understanding of the influence of aqueous phase saturation and chemistry on the IP response (see Vaudelet et al., 2011, for a recent advance in the latter direction based on the coupling of a reactive transport code with a mechanistic IP model);
- (4) the understanding of the influence of non-aqueous phases, and the effect of their wettability with respect to the solid phase, on the IP response (see recent work by Schmutz et al., 2010, and Revil et al., 2011);
- (5) the understanding of the influence of bacteria and biofilms, especially the biological effect versus the associated metallic precipitation effect (electrode polarization) and the potential role of conductive pili, on the IP response;
- (6) the understanding of the IP response of organic material (e.g., plant/tree roots, wood, peat) (see Martin, 2010, and Zanetti et al., 2011, for measurements on oak and tree roots, respectively);
- (7) the understanding of the occurrence of anisotropy in the IP response in dependence on microgeometrical characteristics (see Winchen et al., 2009, for a first synthetic study on the occurrence of anisotropic IP responses);
- (8) the understanding of the effect of ice-water phase transition on the IP response.

Whereas challenges 1-3 are concerning the improvement of theoretical, experimental, and modelling results for well investigated systems, only a limited database exists to date with respect to challenges 4-8.

LABORATORY MEASUREMENTS

Laboratory SIP measurements are required to improve our understanding of the physicochemical controls on the induced polarization effect and test models (theoretical, empirical, mechanistic) for IP source mechanisms. Ward et al. (1995) concluded that laboratory measurements should focus on establishing the dependence of SIP on pore/grain size, surface area, chemistry, saturation, temperature, multiple fluid phases (e.g., water and hydrocarbon) and permeability. As outlined at the end of the previous section, this statement holds today, although some of the above controls have been further investigated in laboratory studies over the past 15 years, including mainly textural parameters (e.g., Vanhala, 1997; Slater and Lesmes, 2002; Scott and Barker, 2003; Binley et al., 2005; Slater et al., 2006; Kruschwitz et al., 2010; Weller et al., 2010a) and permeability (e.g., Börner et al., 1996; Slater and Lesmes, 2002; Binley et al., 2005; Revil and Florsch, 2010; Zisser et al., 2010a; Koch et al., 2011; Revil et al., 2012b). More laboratory measurements are particularly needed regarding the effect of chemistry (e.g., Lesmes and Frye, 2001; Vaudelet et al., 2011; Weller et al., 2011), saturation (e.g., Ulrich and Slater, 2004; Jougnot et al., 2010; Breede et al., 2012), temperature (e.g., Binley et al., 2010; Zisser et al., 2010b; Martinez et al., 2012), multiple fluid phases (e.g., Cassiani et al., 2009; Schmutz et al., 2010; Revil et al., 2011), and in addition effective pressure (e.g., Zisser and Nover, 2009), grain-size distribution (e.g., Revil and Florsch, 2010), pH (e.g., Skold et al., 2011) and the effect of microbial processes (see Atekwana and Slater, 2009, for a recent review). Biogeophysics research has determined that SIP is one of the most promising geophysical techniques for detecting the alteration of mineral-fluid interfaces and pore geometries resulting from microbial growth and biofilm formation (e.g., Abdel Aal et al., 2004; Ntarlagiannis et al., 2005a; Davis et al., 2006; Abdel

Aal et al., 2009, 2010a,b) as well as biomineralization (e.g., Ntarlagiannis et al., 2005b; Williams et al., 2005; Slater et al., 2007; Personna et al., 2008).

There are significant challenges to obtaining accurate and repeatable SIP measurements. Sample preparation procedures require considerable attention to detail if representative measurements of a material are to be obtained. This is a particularly challenging issue for unconsolidated samples, where it is difficult to reliably reproduce the distribution of mineral-fluid interfaces and pores/pore throats controlling the SIP effect. This issue may confound attempts to reproduce SIP responses of natural materials in a specific laboratory, or between laboratories (Figure 4, right). Small differences in column packing and saturation can result in significant changes in SIP spectra between identical soils (Figure 4, left).

The size of the sample holder and details on sample placement (e.g., wet or dry packed, compaction applied, etc.) are important considerations. Sample holders that are too small may prevent inclusion of larger end members of a material grain size distribution, whereas too large sample holders may suffer from inhomogeneous packing. Electrical and physical measurements should be made on the same exact sample using, where possible, multi-function sample holders (e.g., Slater and Lesmes, 2002; Breede et al., 2011), in order to avoid uncertainty associated with differences between samples. Temperature should be recorded and controlled, and the sample should be saturated with appropriate fluids of a specified salinity/composition. Furthermore, the sample should be saturated for sufficient time to ensure chemical equilibrium.

Laboratory SIP measurements are usually based on frequency-domain instruments. Four-electrode measurements are required for low-frequency (< 1 kHz) SIP measurements as

polarization errors are unacceptably large when using two-electrode techniques. However, four-electrode measurements suffer from capacitive coupling above 1 kHz such that some workers combined four- and two-electrode techniques (e.g., Lesmes and Morgan, 2001). Current densities used in SIP measurements should be sufficiently low to avoid non-linear effects. Vanhala and Soininen (1995) did not find a significant change of the SIP response of the samples they investigated in the range from 10^{-5} to 0.2 A/m^2 ; Zimmermann et al. (2008a) did not observe significant non-linear effects either, using current densities between 0.01 and 2 A/m^2 . While potentially more prone to non-linear effects, higher current densities are advantageous in terms of better signal-to-noise ratio (Vanhala and Soininen, 1995) and reduced polarization of the current electrodes (Zimmermann et al., 2008a). Calibration of the instrumentation against resistor-capacitor circuits, water samples and other reference materials is a critical requirement and should be reported. After calibration, or regarding the electrical properties of the measurement system and the sample holder, it is possible to reduce phase errors to $\pm 0.1 \text{ mrad}$ for frequencies between 1 mHz and 1 kHz (Zimmermann et al., 2008a). To validate the accuracy of the measuring apparatus, the IP working group of the German Geophysical Society has developed a set of reference materials and devices that is available to research institutions (Figure 4, right).

Ward et al. (1995) stated that more work on the effects of electrode material was needed. However, consensus is emerging regarding electrode construction and placement for SIP measurements. Non-polarizing potential electrodes are not a strict requirement of modern instruments where input impedances are large ($> 100 \text{ M}\Omega$), although their use favours accurate phase measurements. Most critical is to remove the metal potential electrode from the current path, by placing it in electrolytic contact at the edge of the current flow (Vinegar and Waxman, 1984). Metal electrodes in the current path can generate spurious phase effects

exceeding 10 mrad as a result of a potential gradient along the electrode (Vanhala and Soininen, 1995). Unsaturated measurements are challenging as novel methods to avoid metallic electrodes embedded in the soil are required. Ulrich and Slater (2004) placed electrodes in ceramic porous frits whereas others used gels to assure electrolytic contact (Binley et al., 2005). Point and ring potential electrodes have both been used. In the case of sample heterogeneity, a point electrode could record a bias due to deviations from 1D current flow. Ring electrodes overcome this as they integrate the electric field around the circumference of a sample holder. However, significant phase errors develop if a gradient in potential exists around the ring. Ring electrodes should therefore be used with caution. Another critical point is the distance between the outer current electrodes to the inner potential electrodes. In case of directly coupled current electrodes, like plates, the distance between current electrode and potential electrode on each side should be at least twice the sample width to avoid errors associated with the polarization of the current electrodes (Zimmermann et al., 2008a). However, a larger distance between current and potential electrodes should also be avoided due to the increase of measurement error if the sample resistance between current and potential electrodes becomes larger than the sample resistance between the two potential electrodes (Zimmermann et al., 2008a).

The recent advent of SIP imaging systems with high phase-accuracy (e.g., Zimmermann et al., 2008b) is bringing new challenges to laboratory SIP research. Maintaining sufficiently low contact resistance without causing polarization errors on a large array of electrodes is a substantial issue. Like the four-electrode systems, the validation of imaging systems requires embedding targets with a known complex resistivity response within the imaging vessel. Appropriate image reconstruction (inversion) techniques are also required to advance this research (see next section).

Although aspects of laboratory SIP acquisition remain uncertain, some general conclusions can be drawn from the review presented here. Procedures for sample preparation, instrument calibration and testing should be fully documented. We recommend that researchers adopt established procedures for sample preparation developed for engineering tests when appropriate. Finally, the physical and chemical characteristics of the sample should be tabulated in publications, as this will assist efforts directed towards validating models.

MODELLING AND IMAGING

Ward et al. (1995) emphasized the need for ‘fast’ forward and inverse models and encouraged the development of 3D codes for IP applications. They also highlighted the need for incorporation of electromagnetic (EM) coupling effects within the modelling codes and recognized the need for accounting for noise in imaging tools. These recommendations still hold today, although there has been, over the past ten years, an increase in the number of imaging codes (commercial and academic) that can model IP data. This has been partly driven by the wider availability of relatively low cost IP field instruments, but also because of the greater appreciation of the potential value of IP for characterization of the subsurface.

Many of the current IP imaging codes follow the chargeability formulation of Seigel (1959) and model data in the time domain (e.g., Oldenburg and Li, 1994; Li and Oldenburg, 2000; Chambers et al., 2004). These tools permit, through linear approximations, rapid assessment of 2D and 3D images of the subsurface. This, now classical, formulation can be extremely effective in delineation of chargeable bodies within the subsurface but is limited for

quantitative studies that attempt to link petrophysical models derived from frequency-domain (SIP) data. Thus, we find that the main challenge today for IP modelling and imaging (inversion with fine pixel/voxel parameterization) arises from the demand to use the method as a quantitative tool for structure and process characterization, imposing highest requirements on accuracy rather than speed alone.

With the increasing focus on SIP measurements given their superior diagnostic capability, frequency-domain modelling formulations in terms of complex resistivity (e.g., Kemna and Binley, 1996; Weller et al., 1996; Shi et al., 1998) have become more attractive and complex resistivity inversion algorithms have been developed (e.g., Kemna and Binley, 1996; Shi et al., 1998; Kemna, 2000; Blaschek et al., 2008) and used in a variety of laboratory (e.g., Kemna et al., 2000; Zimmermann et al., 2008b) and field (e.g., Kemna et al., 2004; Slater and Binley, 2003, 2006; Hördt et al., 2007, 2009; Williams et al., 2009; Flores Orozco et al., 2011) applications, one example being shown in Figure 5. These schemes assume quasi-static electric and magnetic fields, i.e., EM coupling effects, typically occurring above 100 Hz (Figure 6), are not accounted for. Consequently, only low-frequency (< 100 Hz) or decoupled datasets can be processed with these schemes without larger systematic errors. Recently, Commer et al. (2011) developed a complex resistivity inversion code based on full EM modelling where both IP and EM coupling effects are accounted for. With the availability of such tools, the inversion of broadband SIP field data will become possible in the future.

Another current limitation is the assumption of isotropic IP parameters in the available modelling and inversion algorithms. Winchen et al. (2009) recently demonstrated that the effective SIP response of statistically distributed two-component mixtures with underlying isotropic Cole-Cole relaxation properties generally becomes anisotropic (and potentially

bimodal), and that the characteristic structural properties of the mixture (volume fraction, correlation length of the statistical distribution) can be inferred from the anisotropic response using inverse modelling. An anisotropic SIP response has also been reported in recent laboratory studies (e.g., Zisser and Nover, 2009; Weller et al., 2010b). This indicates that anisotropy might be necessary to consider in many field studies, but also that it contains exploitable structural information. While the extension of complex resistivity modelling to the anisotropic case is straightforward (Kenkel et al., 2012), anisotropic complex resistivity inversion will be challenged by the high degrees of freedom of the model, which will require special regularization approaches, as already known from anisotropic DC resistivity inversion (Herwanger et al., 2004).

One of the most crucial issues in quantitative IP imaging is, like in any inversion, the correct description of data errors and the right degree of data fitting (Figure 7). Despite clear recognition of this in Ward et al. (1995), this aspect of IP imaging is widely overlooked. Over-fitting the data (corresponding to underestimating the data error) should be avoided, because this typically leads to artefacts in the images (Figure 7a), as should under-fitting (overestimating the data error), which results in images with non-optimal resolution and contrast (Figure 7c). Many schemes are being used for quantitative imaging purposes, which seek for the minimization of data misfit instead of the optimization of some regularization function (usually minimization of model roughness) subject to fitting the data to a well-defined degree. We point out that such schemes are not only prone to the creation of artefacts in space – often mistaken as evidence of high spatial resolution – but are generally unsuitable for the inversion of time-lapse data due to inconsistent data fitting at individual time steps and the related creation of spatio-temporal artefacts. Slater and Binley (2006) demonstrated how IP data error can be estimated using normal and reciprocal measurements. Flores Orozco

et al. (2012a) recently proposed an extended approach, where the IP data error is determined as a function of resistance. We note in this context that normal-reciprocal discrepancy does not necessarily vanish if the underlying IP effect is of non-linear nature; however, normal-reciprocal discrepancy might then be indicative of modelling error, because non-linear IP is not accounted for in the implemented Poisson equation, and thus still be useful to weight the misfit between measured and predicted data in the inversion.

The inversion of SIP datasets obviously turns a 2-D or 3-D inverse problem in space into an overall 3-D or 4-D inverse problem, respectively, if the ‘spectral’ parameterization is based on some regular frequency sampling. In particular if fine parameterizations are used, as generally the case with respect to space in tomographic applications, computationally expensive numerical problems result. The computational burden becomes even worse when time-lapse spectral data are to be inverted, potentially manifesting a 5-D inverse problem (3-D space, signal frequency, experimental time). Computational limitations will therefore imply the use of alternative, sparser parameterizations. With respect to space, parameters may be grouped into lithological zones (which one may refer to as ‘parametric’ inversion) – based on *a priori* information – in which variability could be allowed to follow some pre-defined correlation structure by corresponding regularization approaches (e.g., Maurer et al., 1998; Linde et al., 2006). To reduce the number of parameters describing the spectral response, available petrophysical IP models (empirical or mechanistic) may be incorporated into the inversion. Such an approach has already been demonstrated in several publications, for example, on the basis of the phenomenological Cole-Cole model (Yuval and Oldenburg, 1997; Routh et al., 1998; Loke et al., 2006), reducing the number of parameters with respect to the frequency dimension to four (DC resistivity, chargeability, time constant, frequency exponent). The approach may be extended, for example, by assuming a certain number of

Cole-Cole relaxation terms or a superposition of Debye models according to a general, rather finely sampled distribution of relaxation times (e.g., Morgan and Lesmes, 1994; Nordsiek and Weller, 2008; Zisser et al., 2010a). However, while the latter parameterization takes some fundamental physical relaxation behaviour into account, it does not mean an effective reduction of parameter space and will generally also require some sort of regularization (with respect to the relaxation time distribution). Similarly, for the inversion of time-lapse IP data, a reduced parameterization on the basis of a process model would be desirable – such as being pursued for time-lapse resistivity inversion in the field of hydrogeophysics (see, e.g., Ferré et al., 2009). However, for applications like the monitoring of biogeochemical system transformations such models are still far from being available. Alternatively, simple ‘difference inversion’ schemes (LaBrecque and Yang, 2001) or even full time-lapse inversion schemes (Kim et al., 2009; Karaoulis et al., 2011a) should be adopted to reduce the influence of systematic errors (in both the forward modelling and the data). A first full time-lapse inversion scheme for complex resistivity data was recently developed by Karaoulis et al. (2011b), which represents a significant advancement regarding the inversion of time-lapse SIP data.

The above parameterization aspects are directly linked with the issue of regularization in IP inversion. We recommend the development of inversion schemes that are capable of incorporating any sort of *a priori* information and other available data (geophysical, hydrogeological, biogeochemical) to constrain the inversion in a flexible manner. Such flexibility may be provided in a stochastic formulation of the inverse problem, using an *a priori* model covariance matrix for regularization, if available.

Equally challenging is the need to provide reliable estimates of uncertainty in IP/SIP imaging codes. The propagation of data error, modelling error, errors in the petrophysical models and non-uniqueness in the inverse solutions may lead to images with significantly high uncertainty. As we continue to ‘stretch’ the potential value of IP by examining (sometimes) extremely subtle contrasts in subsurface bodies, we need to recognize and quantify uncertainty in the resulting models. Attempts to assess uncertainty of inverted parameters of IP relaxation models (e.g., Ghorbani et al., 2007; Chen et al., 2008) show promising results and we anticipate rapid growth in this area and hopeful proliferation through to imaging tools.

FIELD MEASUREMENTS

The recommendations for IP research detailed in Ward et al. (1995) focused primarily on mining and environmental problems. While both remain active research areas, the latter has seen a dramatic increase in the type of problems studied, as well as detailed investigation of the mechanisms underlying the IP effect. Particularly active areas of environmental research include application of IP techniques for studying problems in hydrogeology, agriculture and biogeochemistry (Slater, 2007; Atekwana and Slater, 2009). Mining relevant problems continue to focus on economic mineral discrimination, an increasingly important topic given surging demand for both base and precious metals.

Field-scale application of the IP technique for quantifying subsurface hydraulic properties is perhaps the most significant application development since Ward et al. (1995) (Börner et al., 1996; Kemna, 2000; Slater and Glaser, 2003; Kemna et al., 2004; Hördt et al., 2007, 2009),

having relevance to numerous problems where hydrologic processes are of interest. Growing interest in the use of SIP field methods to assess mineralogical and geochemical properties related to subsurface microbial activity represents another significant development in SIP research (Williams et al., 2009; Flores Orozco et al., 2011), largely spawning the sub-discipline of biogeophysics. It is worth noting that many aspects of the aforementioned research are inextricably linked, with differences in mineral and fluid composition related to variations in lithology and hydrological properties. New areas of IP field applications do also include archaeological prospection (Schleifer et al., 2002; Weller et al., 2006; Florsch et al., 2011).

The recent spate of laboratory studies correlating hydrological and biogeochemical properties with a characteristic spectral response strongly suggests that field SIP datasets have inherent value for improving estimates of parameters needed for subsurface characterization and monitoring (e.g., pore/grain size, permeability, surface area, fluid chemistry, mineral precipitation etc.). Although time consuming and – under certain circumstances – offering only modest improvements over measurements of bulk polarization (as measured in standard time-domain IP surveys), future research must be focused on extracting meaningful information from a growing number of field SIP datasets. Recent field SIP imaging results (Figure 8) are sufficiently encouraging to warrant such research, with frequency-dependent phase anomalies found to correlate well with both hydrogeologic properties (Figure 9), hydrocarbon contaminant concentration (Flores Orozco et al., 2012b), and subsurface microbial activity (Williams et al., 2009; Flores Orozco et al., 2011).

Certainly, the ability to unambiguously decouple the myriad of source mechanisms underlying SIP anomalies (e.g., the overlapping contributions of biogeochemistry, hydrology

and lithology) remains challenging; however, the potential of SIP techniques for localizing areas of interest and providing unique insight into the nature of the underlying responses supports continued research. Discrimination of IP source mechanisms was a recurrent theme in the recommendations of Ward et al. (1995), and successful source discrimination will only prove tractable by combining sufficiently constrained datasets, comprised of geophysical, geochemical, mineralogical and hydrological information. In the absence of such constraints, over-interpretation – or worse – misinterpretation of SIP datasets may result.

One means for improving SIP data quality and promoting consistency in inversion/imaging results is the development of a field protocol that can be followed by experimentalists and contractors. While far from exhaustive, we identify some of the more critical aspects of such a protocol:

1. Reciprocal measurements are critical for assessing the quality of field data, being far more valuable than repeat measurements at a given dipole(s), which are not useful in the case of systematic errors (Slater and Binley, 2006). While time-consuming and incapable of absolutely quantifying systematic errors, reciprocal measurements must be made to assure data quality and enable accurate error estimates, with such data critical for inversion/imaging (see previous section).
2. Development of processing and modelling techniques has effectively minimized the need for specific array designs. Nonetheless, a good starting point remains the dipole-dipole array to minimize electrode polarization (avoid current injection before taking potential readings at an electrode) and EM coupling, provided that signal-to-noise ratios are acceptable. The dipole-dipole array also facilitates the use of multi-channel instruments.

3. A variety of metal and metal-metal salt (i.e., non-polarizing (NP) electrodes) have been shown to provide field data of acceptable quality over a range of acquisition frequencies (LaBrecque and Dailey, 2008). As with stainless steel electrodes, the use of NP electrodes as both transmitting and receiving electrodes requires an appropriate acquisition strategy in order to avoid poor data reciprocity (Dahlin et al., 2002). At low current, however, it is recommended that NP electrodes be used as both transmitting and receiving electrodes given their excellent data reciprocity and rapid return to rest potentials post-current injection (Figure 10). Low-drift NP electrodes may also be critical for data collection at very low frequencies (< 0.01 Hz) to avoid distortions of the voltage signal which are difficult to filter out.
4. The issue of capacitive coupling can represent a significant problem at frequencies > 10 Hz. Use of individual, shielded cables connecting each electrode can minimize coupling effects, and their use – while cumbersome and an added expense – is important for high-quality, high-frequency data. Systems where cable-coupling issues are compensated for through equipment design renders this issue moot (Zimmermann et al., 2008b).
5. Alternatively, capacitive coupling can be reduced through the use of remote units situated close to the electrodes, which transfer digitized data through an optical link. Compensation techniques may still be necessary to reduce coupling through the transmitter cable (Radic, 2004). The remote units and the additional cable make such a system relatively expensive and cumbersome to use, but potentially unavoidable if accurate data at high frequencies are required.
6. Development of a ‘standardized’ post-acquisition data handling strategy is needed to enable comparison of SIP data collected at various sites, including the following: definition of outliers to be removed prior to inversion, implementation of an

appropriate error model (Flores Orozco et al., 2012a), and removal of EM effects (e.g., Kemna et al., 1999; Ghorbani et al., 2009).

Although challenges remain in resolving issues related to field SIP data acquisition, processing and interpretation, several important conclusions can be drawn. First and foremost, it is agreed that SIP datasets will most likely provide insight into ‘patterns’ of subsurface properties useful for conditioning reactive transport models rather than providing an accurate pixel-by-pixel map of specific properties of interest (e.g., hydraulic conductivity, mineral enrichment, bulk subsurface redox status, etc.). Such an accomplishment should not be discounted, as delineation of patterns over field dimensions (10’s to 100’s m) and their correlation to properties of interest is a significant improvement over current approaches, which are almost exclusively constrained by direct sampling. Second, it is recognized that care must be taken in collecting time-domain field measurements designed to replicate frequency-domain laboratory measurements, such that data are recorded at sufficiently high rates (i.e., sufficient time windows) to capture the expected polarization phenomena. Third, normalization of data acquisition approaches and assessment of data errors prior to inversion should better facilitate comparison of results obtained as part of a growing number of field SIP datasets.

CONCLUSIONS

In this article we summarized the state of the science and the perspectives of the spectral induced polarization method for near-surface applications as reflected by the outcome of

intense discussions held among leading researchers in the field at the recent international IP workshop in Bonn, Germany.

Considerable progress has been made over the last decade in the understanding of the microscopic mechanisms of IP; however, the development of integrated mechanistic models involving the different possible polarization processes at the grain/pore scale remains a challenging task. Such models are required to establish constitutive relationships at the scale of effective IP properties, which are measured in the field, and take understanding of IP signatures beyond the stage of empiricism. Especially important is the case-by-case quantification of the importance of each IP-generating mechanism, in order to derive useful information from the measured IP signals.

With the advances in IP modelling and inversion algorithms, in particular those formulated in the frequency domain (complex resistivity), the improved understanding of SIP signatures inferred from the numerous recent laboratory studies can now be exploited in field applications. However, the integral inversion of 3-D, time-lapse and multi-frequency IP data, defining a 5-D inverse problem (3-D space, signal frequency, experimental time), and the understanding of image resolution and uncertainty with respect to spectral characteristics are still major goals for the future. This also holds for the inclusion of the full electromagnetic equations in the modelling, in order to overcome spectral limitations associated with EM coupling effects masking the higher-frequency SIP response, as well as for the inclusion of available *a priori* information in flexible inversion schemes.

We believe that the SIP method, by combining the diagnostic advantages of spectroscopy and the spatial resolution benefits of a geophysical field method, in particular when applied in an

imaging framework and if the above-stated measurement guidelines are followed, offers potential for subsurface structure and process characterization. The most promising near-surface applications include hydrogeophysical and biogeophysical studies, where SIP may be established as a routine, non-invasive characterization and monitoring tool allowing direct access to textural, hydraulic and/or biogeochemical information.

ACKNOWLEDGMENTS

Andreas Kemna gratefully acknowledges financial support by the SFB/TR 32 ‘Patterns in Soil-Vegetation-Atmosphere Systems: Monitoring, Modelling and Data Assimilation’ funded by the Deutsche Forschungsgemeinschaft (DFG) to organize the International Workshop on Induced Polarization in Near-Surface Geophysics on Sep 30/Oct 1, 2009 in Bonn, which initiated the work on this article. Lawrence Berkeley National Laboratory is operated for the U.S. Department of Energy by the University of California under contract DE-AC02-05CH11231 and Cooperative Agreement DE-FC02ER63446.

REFERENCES

Abdel Aal, G.Z., Atekwana, E.A., Slater, L.D., and Atekwana, E.A., 2004. Effects of microbial processes on electrolytic and interfacial electrical properties of unconsolidated sediments: *Geophysical Research Letters*, 31, L12505, doi:10.1029/2004GL020030.

Abdel Aal, G., Atekwana, E., Radzikowski, S., and Rossbach, S., 2009. Effect of bacterial adsorption on low frequency electrical properties of clean quartz sands and iron-oxide coated sands: *Geophysical Research Letters*, 36, L04403, doi:10.1029/2008GL036196.

Abdel Aal, G.Z., Atekwana, E.A., Rossbach, S., and Werkema, D.D., 2010a. Sensitivity of geoelectrical measurements to the presence of bacteria in porous media: *Journal of Geophysical Research*, 115, G03017, doi:10.1029/2009JG001279.

Abdel Aal, G.Z., Atekwana, E.A., and Atekwana, E.A., 2010b. Effect of bioclogging in porous media on complex conductivity signatures: *Journal of Geophysical Research*, 115, G00G07, doi:10.1029/2009JG001159.

Alvarez, R., 1973. Complex dielectric permittivity in rocks: A method for its measurement and analysis: *Geophysics*, 38, 920-940.

Atekwana, E.A., and Slater, L.D., 2009. Biogeophysics: A new frontier in Earth science research: *Reviews of Geophysics*, 47, RG4004, doi:10.1029/2009RG000285.

Binley, A., Slater, L., Fukes, M., and Cassiani, G., 2005. The relationship between spectral induced polarization and hydraulic properties of saturated and unsaturated sandstone: *Water Resources Research*, 41, W12417, doi:10.1029/2005WR004202.

Binley, A., Kruschwitz, S., Lesmes, D., and Kettridge, N., 2010. Exploiting the temperature effects on low frequency electrical spectra of sandstone: A comparison of effective diffusion path lengths: *Geophysics*, 75, A43-A46.

Blaschek, R., Hördt, A., and Kemna, A., 2008. A new sensitivity-controlled focusing regularization scheme for the inversion of induced polarization data based on the minimum gradient support: *Geophysics*, 73, F45-F54.

Blaschek, R., and Hördt, A., 2009. Numerical modelling of the IP effect at the pore scale: *Near Surface Geophysics*, 7, 579-588.

Börner, F.D., Schopper, J.R., and Weller, A., 1996. Evaluation of transport and storage properties in the soil and groundwater zone from induced polarization measurements: *Geophysical Prospecting*, 44, 583-601.

Breede, K., Kemna, A., Esser, O., Zimmermann, E., Vereecken, H., and Huisman, J.A., 2011. Joint measurement setup for determining spectral induced polarization and soil hydraulic properties: *Vadose Zone Journal*, 10, 716-726.

Breede, K., Kemna, A., Esser, O., Zimmermann, E., Vereecken, H., and Huisman, J.A., 2012. Spectral induced polarization measurements on variably saturated sand-clay mixtures: *Near Surface Geophysics*, *this issue*.

Cassiani, G., Kemna, A., Villa, A., and Zimmermann, E., 2009. Spectral induced polarization for the characterization of free-phase hydrocarbon contamination of sediments with low clay content: *Near Surface Geophysics*, 7, 547-562.

Chambers, J.E., Loke, M.H., Ogilvy, R.D., and Meldrum, P.I., 2004. Noninvasive monitoring of DNAPL migration through a saturated porous medium using electrical impedance tomography: *Journal of Contaminant Hydrology*, 68, 1-22.

Chelidze, T.L., and Gueguen, Y., 1999. Electrical spectroscopy of porous rocks: A review – I. Theoretical models: *Geophysical Journal International*, 137, 1-15.

Chen, Y., and Or, D., 2006. Geometrical factors and interfacial processes affecting complex dielectric permittivity of partially saturated porous media: *Water Resources Research*, 42, W06423, doi:10.1029/2005WR004744.

Chen, J., Kemna, A., and Hubbard, S.S., 2008. A comparison between Gauss-Newton and Markov-chain Monte Carlo-based methods for inverting spectral induced-polarization data for Cole-Cole parameters: *Geophysics*, 73, F247-F259.

Chen, J., Hubbard, S.S., Williams, K.H., Flores Orozco, A., and Kemna, A., 2012. Estimating the spatiotemporal distribution of geochemical parameters associated with biostimulation using spectral induced polarization data and hierarchical Bayesian models: *Water Resources Res.*, 48, W05555, doi:10.1029/2011WR010992.

Commer, M., Newman, G.A., Williams, K.H., and Hubbard, S.S., 2011. 3D induced-polarization data inversion for complex resistivity: *Geophysics*, 76, F157-F171.

Dahlin, T., Leroux, V., and Niessen, J., 2002. Measuring techniques in induced polarization imaging: *Journal of Applied Geophysics*, 50, 279-298.

Davis, C.A., Atekwana, E., Atekwana, E., Slater, L., Rossbach, S., and Mormile, M.R., 2006. Microbial growth and biofilm formation in geologic media is detected with complex conductivity measurements: *Geophysical Research Letters*, 33, L18403, doi:10.1029/2006GL027312.

Dukhin, S.S., and Shilov, P., 1974. Dielectric phenomena and the double layer in disperse systems and polyelectrolytes: John Wiley & Sons, Inc., New York.

Ferré, T., Bentley, L., Binley, A., Linde, N., Kemna, A., Singha, K., Holliger, K., Huisman, J.A., and Minsley, B., 2009. Critical steps for the continuing advancement of hydrogeophysics: *Eos Transactions of the American Geophysical Union*, 90(23), doi:10.1029/2009EO230004.

Fixman, M., 1980. Charged macromolecules in external fields. I. The sphere: *Journal of Chemical Physics*, 72, 5177-5186.

Flores Orozco, A., Williams, K.H., Long, P.E., Hubbard, S.S., and Kemna, A., 2011. Using complex resistivity imaging to infer biogeochemical processes associated with bioremediation of an uranium-contaminated aquifer: *Journal of Geophysical Research*, 116, G03001, doi:10.1029/2010JG001591.

Flores Orozco, A., Kemna, A., and Zimmermann, E., 2012a. Data error quantification in spectral induced polarization imaging: *Geophysics*, 77, E227-E237.

Flores Orozco, A., Kemna, A., Oberdörster, C., Zschornack, L., Leven, C., Dietrich, P., and Weiss, H., 2012b. Delineation of subsurface hydrocarbon contamination at a former hydrogenation plant using spectral induced polarization imaging: *J. Cont. Hydrol.*, *in press*.

Florsch, N., Llubes, M., Téreygeol, F., Ghorbani, A., and Roblet, P., 2011. Quantification of slag heap volumes and masses through the use of induced polarization: application to the Castel-Minier site: *Journal of Archaeological Science*, 38, 438-451.

Ghorbani, A., Camerlynck, C., Florsch, N., Cosenza, P., and Revil, A., 2007. Bayesian inference of the Cole-Cole parameters from time and frequency-domain induced polarization: *Geophysical Prospecting*, 55, 589-605.

Ghorbani, A., Camerlynck, C., and Florsch, N., 2009. CR1Dinv: A Matlab program to invert 1D spectral induced polarization data for the Cole-Cole model including electromagnetic effects: *Computers and Geosciences*, 35, 255-266.

Herwanger, J.V., Pain, C.C., Binley, A., De Oliveira, C.R.E., and Worthington, M.H., 2004. Anisotropic resistivity tomography: *Geophysical Journal International*, 158, 409-425.

Hördt, A., Blaschek, R., Kemna, A., and Zisser, N., 2007. Hydraulic conductivity estimation from induced polarization data at the field scale – the Krauthausen case history: *Journal of Applied Geophysics*, 62, 33-46.

Hördt, A., Blaschek, R., Binot, F., Druiventak, A., Kemna, A., Kreye, P., and Zisser, N., 2009. Case histories of hydraulic conductivity estimation with induced polarisation at the field scale: *Near-Surface Geophysics*, 7, 529-545.

Jougnot, D., Ghorbani, A., Revil, A., Leroy, P., and Cosenza, P., 2010. Spectral induced polarization of partially saturated clay-rocks: A mechanistic approach: *Geophysical Journal International*, 180, 210-224.

Karaoulis, M., Kim, J.-H., and Tsourlos, P.I., 2011a. 4D active time constrained inversion: *Journal of Applied Geophysics*, 73, 25-34.

Karaoulis, M., Revil, A., Werkema, D.D., Minsely, B.J., Woodruff, W.F., and Kemna, A., 2011b. Time-lapse three-dimensional inversion of complex conductivity data using an active time constrained (ATC) approach: *Geophysical Journal International*, 187, 237-251.

Kemna, A., and Binley, A., 1996. Complex electrical resistivity tomography for contaminant plume delineation: *Proceedings of the 2nd Meeting on Environmental and Engineering Geophysics*, Environmental and Engineering Geophysical Society – European Section, 196-199.

Kemna, A., Räckers, E., and Dresen, L., 1999. Field applications of complex resistivity tomography: *Expanded Abstracts of the 69th Annual International Meeting, Society of Exploration Geophysics*, 331-334.

Kemna, A., 2000. Tomographic inversion of complex resistivity – theory and application: Ph.D. thesis, Ruhr-University of Bochum.

Kemna, A., Binley, A., Ramirez, A., and Daily, W., 2000. Complex resistivity tomography for environmental applications: *Chemical Engineering Journal*, 77, 11-18.

Kemna, A., Binley, A., and Slater, L., 2004. Crosshole IP imaging for engineering and environmental applications: *Geophysics*, 69, 97-107.

Kenkel, J., Hördt, A., and Kemna, A., 2012. 2D modelling of induced polarisation data with anisotropic complex conductivities: *Near Surface Geophysics*, *this issue*.

Kim, J.-H., Yi, M.J., Park, S.G., and Kim, J.G., 2009. 4-D inversion of DC resistivity monitoring data acquired over a dynamically changing earth model: *Journal of Applied Geophysics*, 68, 522-532.

Koch, K., Kemna, A., Irving, J., and Holliger, K., 2011. Impact of changes in grain size and pore space on the hydraulic conductivity and spectral induced polarization response of sand: *Hydrology and Earth System Sciences*, 15, 1785-1794.

Kruschwitz, S., Binley, A., Lesmes, D., and Elshenawy, A., 2010. Textural controls on low frequency electrical spectra of porous media: *Geophysics*, 75, WA113-WA123.

Kwon, G.W., Won, Y.S., and Yoon, B.J., 1998. Electrical double-layer interactions of regular arrays of spheres: *Journal of Colloid and Interface Science*, 205, 423-432.

LaBrecque, D.J., and Yang, X., 2001. Difference inversion of ERT data: A fast inversion method for 3-D in situ monitoring: *Journal of Environmental and Engineering Geophysics*, 5, 83-90.

LaBrecque, D., and Daily, W., 2008. Assessment of measurement errors for galvanic-resistivity electrodes of different composition: *Geophysics*, 73, F55-F64.

Leroy, P., Revil, A., Kemna, A., Cosenza, P., and Ghorbani, A., 2008. Complex conductivity of water-saturated packs of glass beads: *Journal of Colloid and Interface Science*, 321, 103-117.

Leroy, P., and Revil, A., 2009. A mechanistic model for the spectral induced polarization of clay materials: *Journal of Geophysical Research*, 114, B10202, doi:10.1029/2008JB006114.

Lesmes, D.P., and Morgan, F.D., 2001. Dielectric spectroscopy of sedimentary rocks: *Journal of Geophysical Research*, 106, 13329-13346.

Lesmes, D.P., and Frye, K.M., 2001. Influence of pore fluid chemistry on the complex conductivity and induced polarization responses of Berea sandstones: *Journal of Geophysical Research*, 106, 4079-4090.

Li, Y., and Oldenburg, D.W., 2000. 3-D inversion of induced polarization data: *Geophysics*, 65, 1931-1945.

de Lima, O.A.L., and Sharma, M.M., 1992. A generalized Maxwell–Wagner theory for membrane polarization in shaly sands: *Geophysics*, 57, 431-440.

Linde, N., Binley, A., Tryggvason, A., Petersen, L.B., and Revil, A., 2006. Improved hydrogeophysical characterization using joint inversion of cross-hole electrical resistance and ground-penetrating radar traveltimes data: *Water Resources Research*, 42, W12404, doi:10.1029/2006WR005131.

Loke, M.H., Chambers, J.E., and Ogilvy, R.D., 2006. Inversion of 2D spectral induced polarization imaging data: *Geophysical Prospecting*, 54, 287-301.

Marshall, D.J., and Madden, T.R., 1959. Induced polarization, a study of its causes: *Geophysics*, 24, 790-816.

Martin, T., 2010. Complex resistivity measurements on oak: *European Journal of Wood and Wood Products*, 70, 45-53.

Martinez, F.J., Batzle, M.L., and Revil, A., 2012. Influence of temperature on seismic velocities and complex conductivity of heavy oil-bearing sands: *Geophysics*, 77, WA19-WA34.

Maurer, H., Holliger, K., and Boerner, D.E., 1998. Stochastic regularization: Smoothness or similarity?: *Geophysical Research Letters*, 25, 2889-2892.

Merriam, J.B., 2007. Induced polarization and surface electrochemistry: *Geophysics*, 72, F157-F166.

Morgan, F.D., and Lesmes, D.P., 1994. Inversion for dielectric relaxation spectra: *Journal of Chemical Physics*, 100, 671-681.

Nordsiek, S., and Weller, A., 2008. A new approach to fitting induced-polarization spectra: *Geophysics*, 73, F235-F245.

Ntarlagiannis, D., Yee, N., and Slater, L., 2005a. On the low-frequency induced polarization of bacterial cells in sands: *Geophysical Research Letters*, 32, L24402, doi:10.1029/2005GL024751.

Ntarlagiannis, D., Williams, K.H., Slater, L., and Hubbard, S., 2005b. Low-frequency electrical response to microbial induced sulfide precipitation: *Journal of Geophysical Research*, 110, G02009, doi:10.1029/2005JG000024.

Oldenburg, D.W., and Li, Y., 1994. Inversion of induced polarization data: *Geophysics*, 59, 1327-1341.

Personna, Y.R., Ntarlagiannis, D., Slater, L., Yee, N., O'Brien, M., and Hubbard, S., 2008. Spectral induced polarization and electrodic potential monitoring of microbially mediated iron sulfide transformations: *Journal of Geophysical Research*, 113, G02020, doi:10.1029/2007JG000614.

Radic, T., 2004. Elimination of cable effects while multi-channel SIP measurements: Proceedings of the 10th European Meeting of Environmental and Engineering Geophysics, European Association of Geoscientists and Engineers, P029.

Revil, A., 1999. Ionic diffusivity, electrical conductivity, membrane and thermoelectric potentials in colloids and granular porous media: A unified model: *Journal of Colloid and Interface Science*, 212, 503-522.

Revil, A., and Cosenza, P., 2010. Comment on “Generalized effective-medium theory of induced polarization” (Michael Zhdanov, 2008, *Geophysics*, 73, F197-F211): *Geophysics*, 75, X7-X9.

Revil, A., and Florsch, N., 2010. Determination of permeability from spectral induced polarization data in granular media: *Geophysical Journal International*, 181, 1480-1498.

Revil, A., Schmutz, M., and Batzle, M.L., 2011. Influence of oil wettability upon spectral induced polarization of oil-bearing sands: *Geophysics*, 76, A31-A36.

Revil, A., 2012. Spectral induced polarization of shaly sands: Influence of the electrical double layer: *Water Resources Research*, 48, W02517, doi:10.1029/2011WR011260.

Revil, A., Karaoulis, M., Johnson, T., and Kemna, A., 2012a. Review: Some low-frequency electrical methods for subsurface characterization and monitoring in hydrogeology: *Hydrogeol. J.*, 20, 617-658.

Revil, A., Koch, K., and Holliger, K., 2012b. Is it the grain size or the characteristic pore size that controls the induced polarization relaxation time of clean sands and sandstones?: *Water Resources Research*, *in press*.

Routh, P.S., Oldenburg, D.W., and Li, Y., 1998. Regularized inversion of spectral IP parameters from complex resistivity data: Expanded Abstracts of the 68th Annual International Meeting, Society of Exploration Geophysicists, 810-813.

Schleifer, N., Weller, A., Schneider, S., and Junge, A., 2002. Investigation of a Bronze Age plankway by spectral induced polarisation: *Archaeological Prospection*, 9, 243-253.

Schmutz, M., Revil, A., Vaudelet, P., Batzle, M., Femenía Viñao, P., and Werkema, D.D., 2010. Influence of oil saturation upon spectral induced polarization of oil-bearing sands: *Geophysical Journal International*, 183, 211-224.

Scott, J.B., and Barker, R.D., 2003. Determining pore-throat size in Permo-Triassic sandstones from low-frequency electrical spectroscopy: *Geophysical Research Letters*, 30, 1450, doi:10.1029/2003GL016951.

Seigel, H.O., 1959. Mathematical formulation and type curves for induced polarization: *Geophysics*, 24, 547-565.

Seigel, H., Nabighian, M., Parasnis, D.S., and Vozoff, K., 2007. The early history of the induced polarization method: *The Leading Edge*, 26, 312-321.

Shi, W., Rodi, W., and Morgan, F.D., 1998. 3-D induced polarization inversion using complex electrical resistivities: Proceeding of the Symposium on the Application of Geophysics to Engineering and Environmental Problems, Environmental and Engineering Geophysical Society, 785-794.

Skold, M., Revil, A., and Vaudelet, P., 2011. The pH dependence of spectral induced polarization of silica sands: Experiment and modeling: Geophysical Research Letters, 38, L12304, doi:10.1029/2011GL047748.

Slater, L., and Lesmes, D.P., 2002. Electrical-hydraulic relationships observed for unconsolidated sediments: Water Resources Research, 38, 1213, doi:10.1029/2001WR001075.

Slater, L., and Binley, A., 2003. Evaluation of permeable reactive barrier (PRB) integrity using electrical imaging methods: Geophysics, 68, 911-921.

Slater, L.D., and Glaser, D.R., 2003. Controls on induced polarization in sandy unconsolidated sediments and application to aquifer characterization: Geophysics, 68, 1547-1558.

Slater L., and Binley, A., 2006. Synthetic and field-based electrical imaging of zero valent iron barrier: Implications for monitoring long-term barrier performance: Geophysics, 71, 129-137.

Slater, L., Ntarlagiannis, D., and Wishart, D., 2006. On the relationship between induced polarization and surface area in metal-sand and clay-sand mixtures: *Geophysics*, 71, A1-A5.

Slater, L., Ntarlagiannis, D., Personna, Y.R., and Hubbard, S.S.M., 2007. Pore-scale spectral induced polarization signatures associated with FeS biomineral transformations: *Geophysical Research Letters*, 34, L21404, doi:10.1029/2007GL031840.

Slater, L., 2007. Near surface electrical characterization of hydraulic conductivity: From petrophysical properties to aquifer geometries – A review, *Surveys in Geophysics*, 28, 169-197.

Sumner, J.S., 1976. Principles of induced polarisation for geophysical exploration: Elsevier, Amsterdam.

Titov, K., Komarov, V., Tarasov, V., and Levitski, A., 2002. Theoretical and experimental study of time domain-induced polarization in water-saturated sands: *Journal of Applied Geophysics*, 50, 417-433.

Ulrich, C., and Slater, L.D., 2004. Induced polarization measurements on unsaturated, unconsolidated sands: *Geophysics*, 69, 762-771.

Vanhala, H., and Soininen, H., 1995. Laboratory technique for measurement of spectral induced polarization response of soil samples: *Geophysical Prospecting*, 43, 655-676.

Vanhala, H., 1997. Mapping oil-contaminated sand and till with the spectral induced polarization (SIP) method: *Geophysical Prospecting*, 45, 303-326.

Vaudelet P., Revil, A., Schmutz, M., Franceschi, M., and Bégassat, P., 2011. Induced polarization signatures of cations exhibiting differential sorption behaviors in saturated sands: *Water Resources Research*, 47, W02526, doi:10.1029/2010WR009310.

Vinegar, H.J., and Waxman, M.H., 1984. Induced polarization of shaly sands: *Geophysics*, 49, 1267-1287.

Ward, S.H., Sternberg, B.K., LaBrecque, D.J., and Poulton, M.M., 1995. Recommendations on IP research: *The Leading Edge*, 14, 243-247.

Weller, A., Seichter, M., and Kampke, A., 1996. Induced-polarization modelling using complex electrical conductivities: *Geophysical Journal International*, 127, 387-398.

Weller, A., Bauerochse, A., and Nordsiek, S., 2006. Spectral induced polarisation – a geophysical method for archaeological prospection in peatlands: *Journal of Wetland Archaeology*, 6, 105-125.

Weller, A., Slater, L., Nordsiek, S., and Ntarlagiannis, D., 2010a. On the estimation of specific surface per unit pore volume from induced polarization: A robust empirical relation fits multiple data sets: *Geophysics*, 75, WA105-WA112.

Weller, A., Nordsiek, S., and Debschütz, W., 2010b. Estimating permeability of sandstone samples by nuclear magnetic resonance and spectral-induced polarization: *Geophysics* 75, E215-E226.

Weller, A., Breede, K., Slater, L., and Nordsiek, S., 2011. Effect of changing water salinity on complex conductivity spectra of sandstones: *Geophysics*, 76, F315-F327.

Williams, K.H., Ntarlagiannis, D., Slater, L.D., Dohnalkova, A., Hubbard, S.S., and Banfield, J.F., 2005. Geophysical imaging of stimulated microbial biomineralization: *Environmental Science and Technology*, 39, 7592-7600.

Williams, K.H., Kemna, A., Wilkins, M.J., Druhan, J., Arntzen, E., N'Guessan, A.L., Long, P.E., Hubbard, S.S., and Banfield, J.F., 2009. Geophysical monitoring of coupled microbial and geochemical processes during stimulated subsurface bioremediation: *Environmental Science and Technology*, 43, 6717-6723.

Winchen, T., Kemna, A., Vereecken, H., and Huisman, J.A., 2009. Characterization of bimodal facies distributions using effective anisotropic complex resistivity: A 2D numerical study based on Cole-Cole models: *Geophysics*, 74, A19-A22.

Wong, J., 1979. An electrochemical model of the induced polarization phenomenon in disseminated sulfide ores: *Geophysics*, 44, 1245-1265.

Yuval and Oldenburg, D.W., 1996. DC resistivity and IP methods in acid mine drainage problems – results from the Copper Cliff mine tailings impoundments: *Journal of Applied Geophysics*, 34, 187-198.

Zanetti, C., Weller, A., Vennetier, M., and Mériaux, P., 2011. Detection of buried tree root samples by using geoelectrical measurements: a laboratory experiment. *Plant and Soil*, 339, 273-283.

Zimmermann, E., Kemna, A., Berwix, J., Glaas, W., Münch, H.M., and Huisman, J.A., 2008a. A high-accuracy impedance spectrometer for measuring sediments with low polarizability: *Measurement Science and Technology*, 19, 105603, doi:10.1088/0957-0233/19/10/105603.

Zimmermann, E., Kemna, A., Berwix, J., Glaas, W., and Vereecken, H., 2008b. EIT measurement system with high phase accuracy for the imaging of spectral induced polarization properties of soils and sediments: *Measurement Science and Technology*, 19, 094010, doi:10.1088/0957-0233/19/9/094010.

Zisser, N., and Nover, G., 2009. Anisotropy of permeability and complex resistivity of tight sandstones subjected to hydrostatic pressure: *Journal of Applied Geophysics*, 68, 356-370.

Zisser, N., Kemna, A., and Nover, G., 2010a. Relationship between low-frequency electrical properties and hydraulic permeability of low-permeability sandstones: *Geophysics*, 75, E131-E141.

Zisser, N., Kemna, A., and Nover, G., 2010b. Dependence of spectral induced polarization response of sandstone on temperature and its relevance to permeability estimation: *Journal of Geophysical Research*, 115, B09214, doi:10.1029/2010JB007526.

FIGURE CAPTIONS

Figure 1: General concept of SIP imaging, also referred to as spectral electrical impedance tomography (EIT), as a geophysical exploration tool which combines the spatial resolution benefits of a tomographic approach (multi-frequency images on the left) with the diagnostic advantages of spectroscopy (spectral response at the pixel/voxel scale on the right), for instance to infer textural, hydraulic or biogeochemical subsurface properties.

Figure 2: A pictorial view of the current conceptualization of the main IP mechanisms, with three types of porous materials characterized by different polarization mechanisms. Type A corresponds to colloidal suspensions for which three polarization mechanisms co-exist (polarization of the Stern and diffuse layers, Maxwell-Wagner polarization). For dense granular media (type B), the diffuse layer is continuous and does not polarize. In the case of type C, both the Stern and diffuse layers are continuous at the scale of the representative elementary volume and therefore do not polarize. Only the membrane polarization and the Maxwell-Wagner polarization co-exist and are influenced by the electrical conductivity in the electrical double layer (this contribution is termed the surface conductivity). From Revil and Cosenza (2010).

Figure 3: Sketch of membrane polarization of a pore sandwiched between two grains. The back diffusion can occur both in the electrical double layer for the counterions and in the bulk pore water for the cations. The accumulation of the salt on one side of the pore diffuses back with a diffusion coefficient that is equal to the mutual diffusion coefficient of the salt. $J_{(+)}^d$ corresponds to the backdiffusion of the counterions of the electrical double layer while J_d corresponds to the backdiffusion of the salt clouds in the pore. From Revil and Cosenza (2010).

Figure 4: (Left) SIP spectra of a sand sample (from an aquifer in Almeria, Spain) acquired intentionally with different sample preparation methods (FZJ: sample highly compacted, BAM-1: sample loosely compacted, BAM-2: sample loosely compacted and use of non-optimized sample holder). (Right) Comparative measurements on BAM reference material over three years at six German institutions. BAM: Federal Institute for Materials Research and Testing, Berlin; TU C: Clausthal Technical Univ.; TU B: Berlin Technical Univ.; TU Bs: Braunschweig Technical Univ.; TU L: Leipzig Univ.; FZJ: Jülich Research Centre; RWTH: Aachen Technical Univ.

Figure 5: Cross-borehole complex conductivity inversion result from the Drigg Low Level Radioactive Waste Disposal Site, Cumbria, UK, showing (a) real component, (b) imaginary component and (c) phase of complex conductivity. Geological logs and natural gamma logs are shown for comparison. Note the complementary information provided by real and imaginary components of complex conductivity, which in conjunction allow clear lithological discrimination. From Kemna et al. (2004).

Figure 6: Apparent resistivity phase spectra contaminated by positive (left) and negative (right) EM coupling. Circles and triangles indicate, respectively, normal and reciprocal dipole-dipole cross-borehole measurements collected in a fluvial aquifer. The thin solid curve shows the phase response of a fitted dual Cole-Cole model, the thick solid curve the response without the EM coupling term. Modified from Kemna et al. (1999).

Figure 7: Cross-sectional resistivity phase images obtained from impedance field data collected at the US Department of Energy's Rifle Integrated Field Challenge site near Rifle, Colorado (USA), using different phase error descriptions in the inversion: (a) constant phase error model with error level obtained from global normal-reciprocal data analysis, (b) error model based on a power-law dependence of phase error upon resistance as obtained from range-wise normal-reciprocal data analysis, (c) constant phase error model with intentionally increased error level relative to (a). All inversions were fitted to an error-weighted root-mean-square value for the phase data misfit of 1. The zone of increased polarizability in (b) coincides with a zone of ongoing biogeochemical processes after acetate injection in the course of **bioremediation of the uranium-contaminated aquifer at the site. The image in (a) contains artefacts since with the used phase error description parts of the data are over-fitted; the image in (c) lacks resolution and contrast because of under-fitting the data due to the use of an overestimated phase error.** Solid circles indicate position of deployed surface electrodes. Modified from Flores Orozco et al. (2011).

Figure 8: Field SIP imaging results (left: resistivity, right: phase) obtained along a 30 m transect at the US Department of Energy's Rifle Integrated Field Challenge site near Rifle, Colorado (USA). Reciprocal data were acquired over the 0.06-16 Hz frequency range using a modified dipole-dipole configuration between 30 equally spaced Cu/CuSO₄ electrodes, with a

dipole spacing of 4 m and a total of 27 potential dipoles per current dipole. See Chen et al. (2012) for further details.

Figure 9: Results from cross-borehole SIP imaging at a site close to the Strasbourg-Entzheim airport (France). Exemplary raw data shown in Figure 6. Left image: IP relaxation time as obtained from post-inversion Cole-Cole model fitting (modified from Kemna et al., 1999). Right image: Hydraulic permeability (in darcies) as estimated from the 0.125 Hz complex resistivity image using the model by Börner et al. (1996) (from Kemna, 2000). Geological log shown for comparison. In the sand-gravel sections, larger relaxation times are observed in the saturated zone than in the vadose zone, indicating larger relaxation lengths in saturated pores. The permeability image in particular delineates the low-permeable clayey silt layer.

Figure 10: (a) Temporal voltage response of a current transmitting dipole with the following specifications: 4 m dipole spacing; Cu/CuSO₄ electrodes; 55 V transmitting voltage; 0.25 Hz. (b) Voltage decay on the same dipole following cessation of current injection; voltage response due to electrode polarization is below 1 mV (relative to background SP response of ~5.7 mV) after ca. 100 seconds.

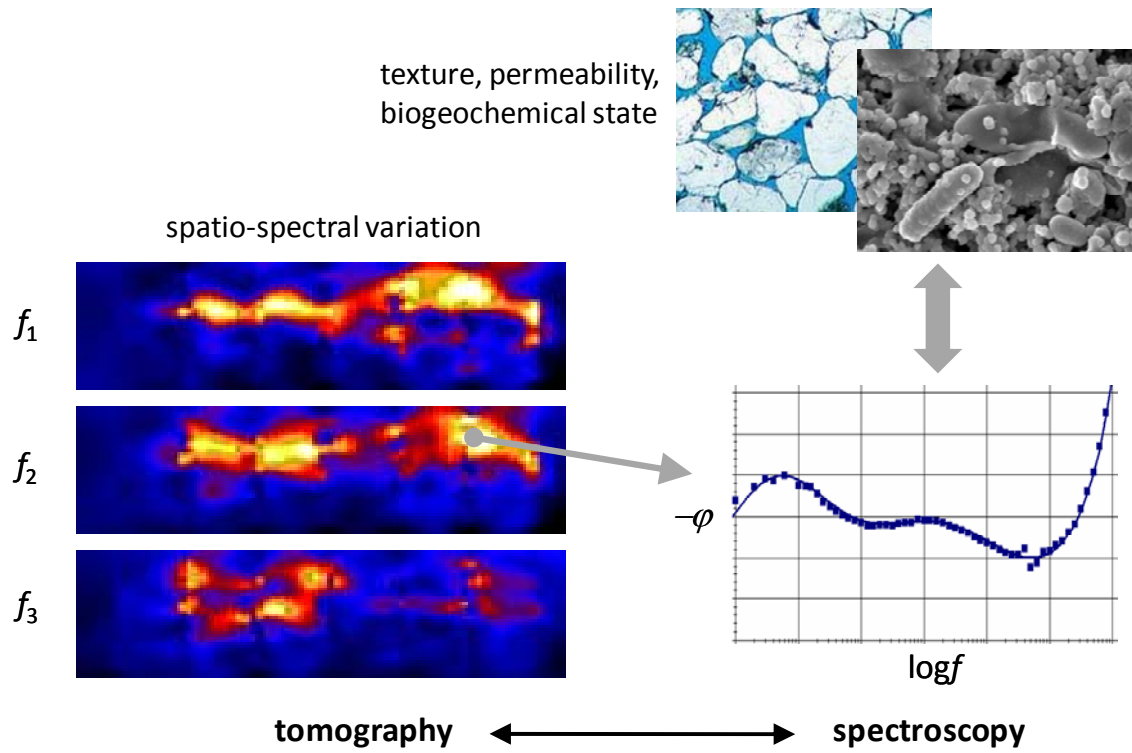


Figure 1: General concept of SIP imaging, also referred to as spectral electrical impedance tomography (EIT), as a geophysical exploration tool which combines the spatial resolution benefits of a tomographic approach (multi-frequency images on the left) with the diagnostic advantages of spectroscopy (spectral response at the pixel/voxel scale on the right), for instance to infer textural, hydraulic or biogeochemical subsurface properties.

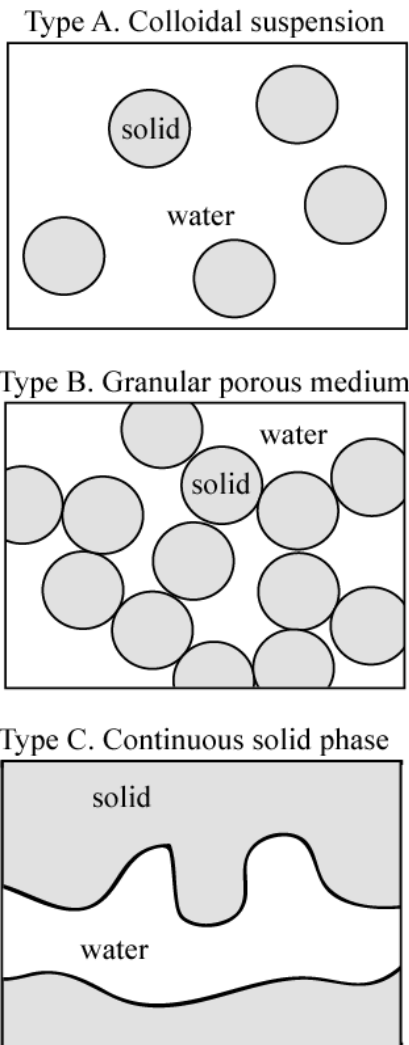


Figure 2: A pictorial view of the current conceptualization of the main IP mechanisms, with three types of porous materials characterized by different polarization mechanisms. Type A corresponds to colloidal suspensions for which three polarization mechanisms co-exist (polarization of the Stern and diffuse layers, Maxwell-Wagner polarization). For dense granular media (type B), the diffuse layer is continuous and does not polarize. In the case of type C, both the Stern and diffuse layers are continuous at the scale of the representative elementary volume and therefore do not polarize. Only the membrane polarization and the Maxwell-Wagner polarization co-exist and are influenced by the electrical conductivity in the electrical double layer (this contribution is termed the surface conductivity). From Revil and Cosenza (2010).

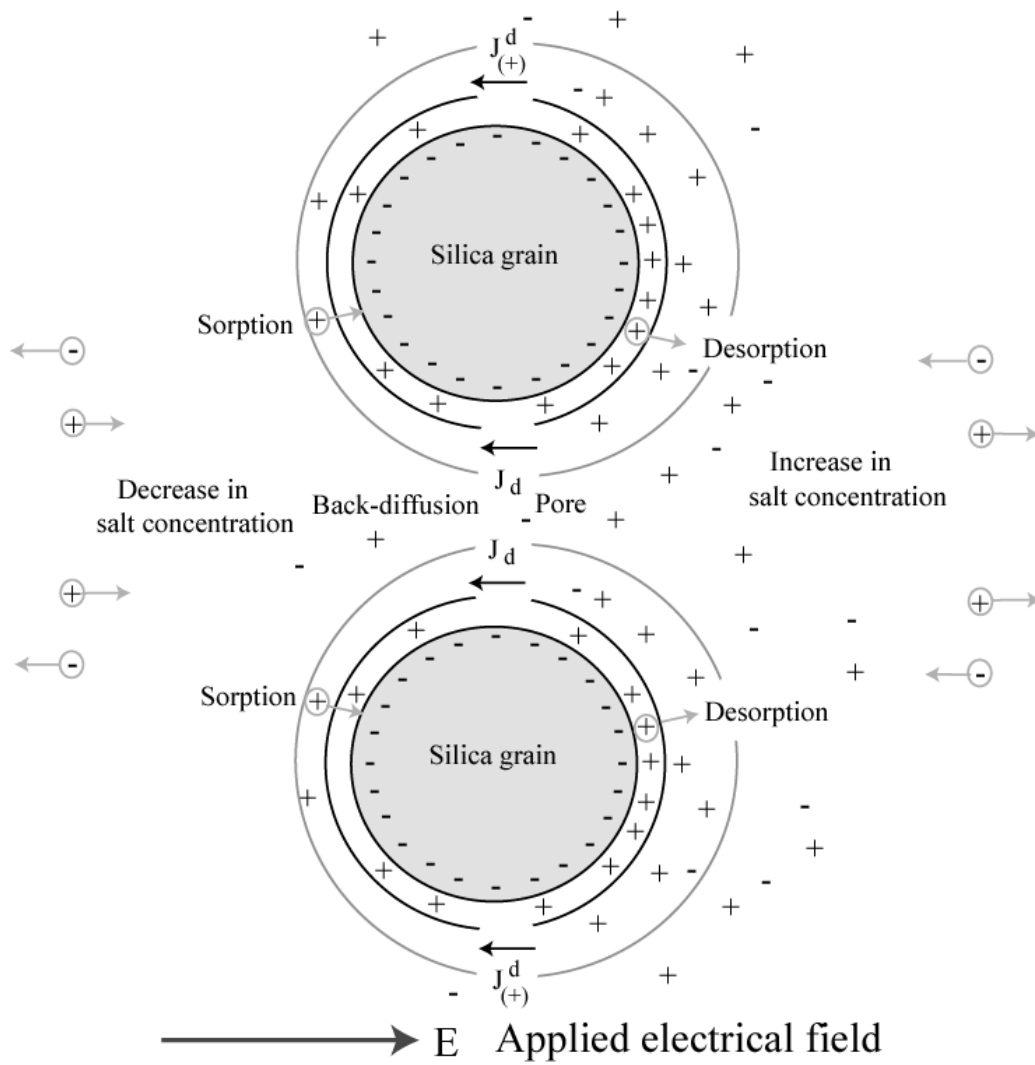


Figure 3: Sketch of membrane polarization of a pore sandwiched between two grains. The back diffusion can occur both in the electrical double layer for the counterions and in the bulk pore water for the coions. The accumulation of the salt on one side of the pore diffuses back with a diffusion coefficient that is equal to the mutual diffusion coefficient of the salt. $J_d^{(+)}$ corresponds to the backdiffusion of the counterions of the electrical double layer while J_d corresponds to the backdiffusion of the salt clouds in the pore. From Revil and Cosenza (2010).

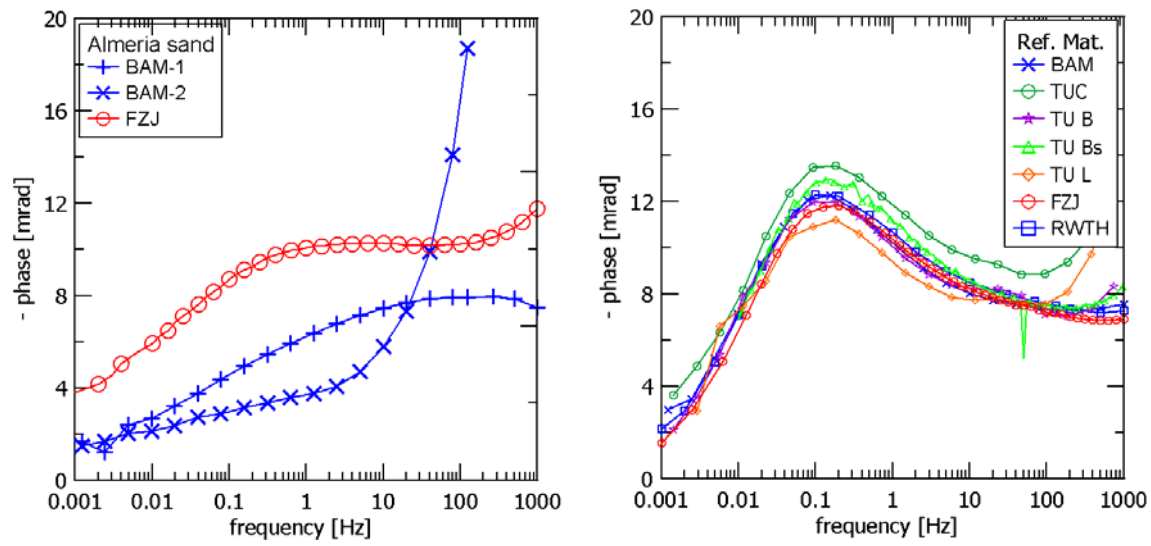


Figure 4: (Left) SIP spectra of a sand sample (from an aquifer in Almeria, Spain) acquired intentionally with different sample preparation methods (FZJ: sample highly compacted, BAM-1: sample loosely compacted, BAM-2: sample loosely compacted and use of non-optimized sample holder). (Right) Comparative measurements on BAM reference material over three years at six German institutions. BAM: Federal Institute for Materials Research and Testing, Berlin; TU C: Clausthal Technical Univ.; TU B: Berlin Technical Univ.; TU Bs: Braunschweig Technical Univ.; TU L: Leipzig Univ.; FZJ: Jülich Research Centre; RWTH: Aachen Technical Univ.

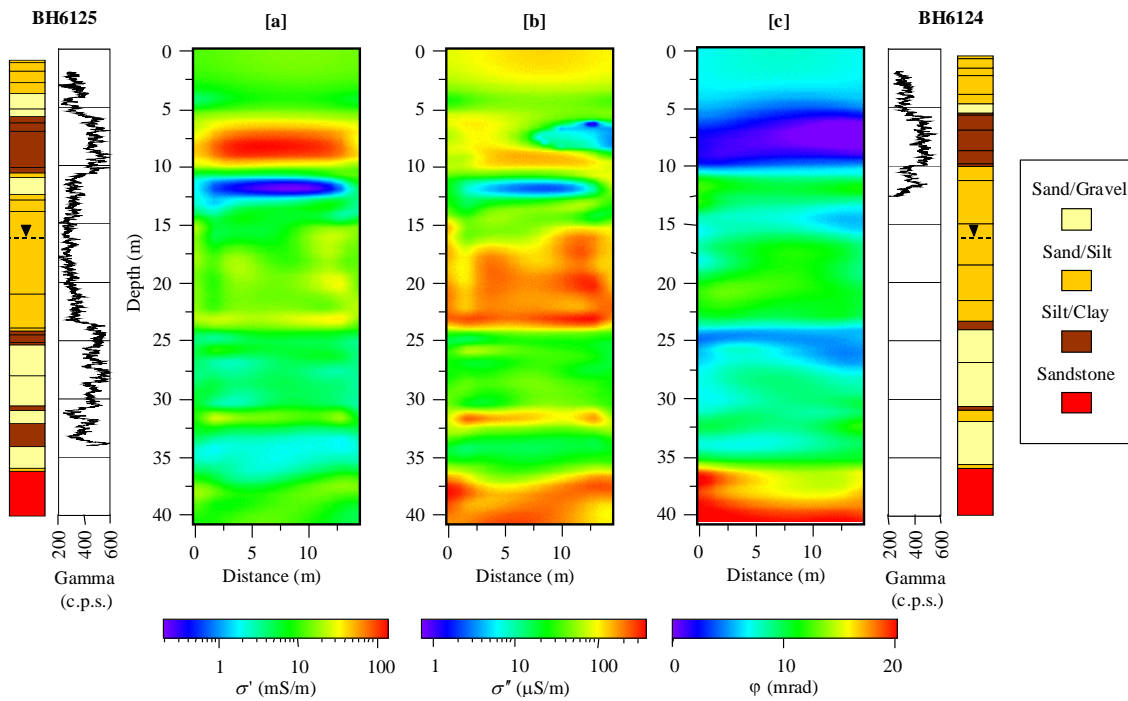


Figure 5: Cross-borehole complex conductivity inversion result from the Drigg Low Level Radioactive Waste Disposal Site, Cumbria, UK, showing (a) real component, (b) imaginary component and (c) phase of complex conductivity. Geological logs and natural gamma logs are shown for comparison. Note the complementary information provided by real and imaginary components of complex conductivity, which in conjunction allow clear lithological discrimination. From Kemna et al. (2004).

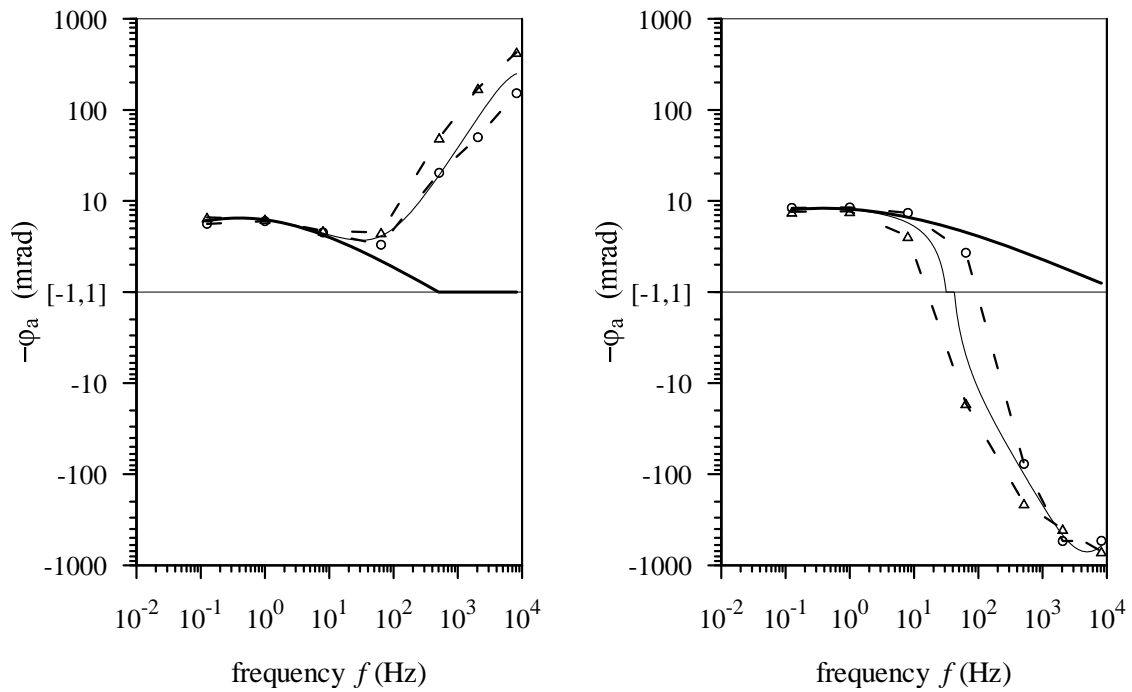


Figure 6: Apparent resistivity phase spectra contaminated by positive (left) and negative (right) EM coupling. Circles and triangles indicate, respectively, normal and reciprocal dipole-dipole cross-borehole measurements collected in a fluvial aquifer. The thin solid curve shows the phase response of a fitted dual Cole-Cole model, the thick solid curve the response without the EM coupling term. Modified from Kemna et al. (1999).

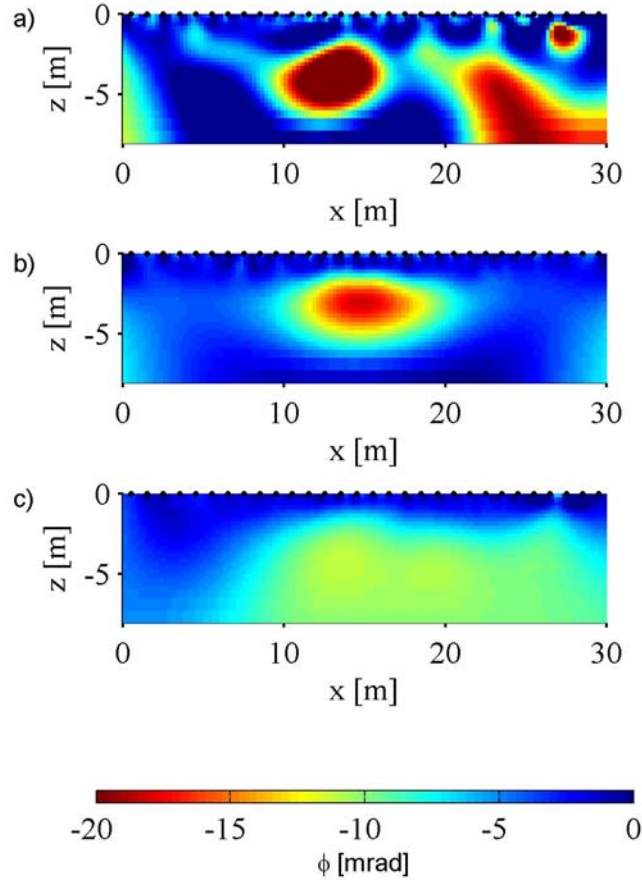


Figure 7: Cross-sectional resistivity phase images obtained from impedance field data collected at the US Department of Energy’s Rifle Integrated Field Challenge site near Rifle, Colorado (USA), using different phase error descriptions in the inversion: (a) constant phase error model with error level obtained from global normal-reciprocal data analysis, (b) error model based on a power-law dependence of phase error upon resistance as obtained from range-wise normal-reciprocal data analysis, (c) constant phase error model with intentionally increased error level relative to (a). All inversions were fitted to an error-weighted root-mean-square value for the phase data misfit of 1. The zone of increased polarizability in (b) coincides with a zone of ongoing biogeochemical processes after acetate injection in the course of **bioremediation of the uranium-contaminated aquifer at the site. The image in (a) contains artefacts since with the used phase error description parts of the data are over-fitted; the image in (c) lacks resolution and contrast because of under-fitting the data due to the use of an overestimated phase error.** Solid circles indicate position of deployed surface electrodes. Modified from Flores Orozco et al. (2011).

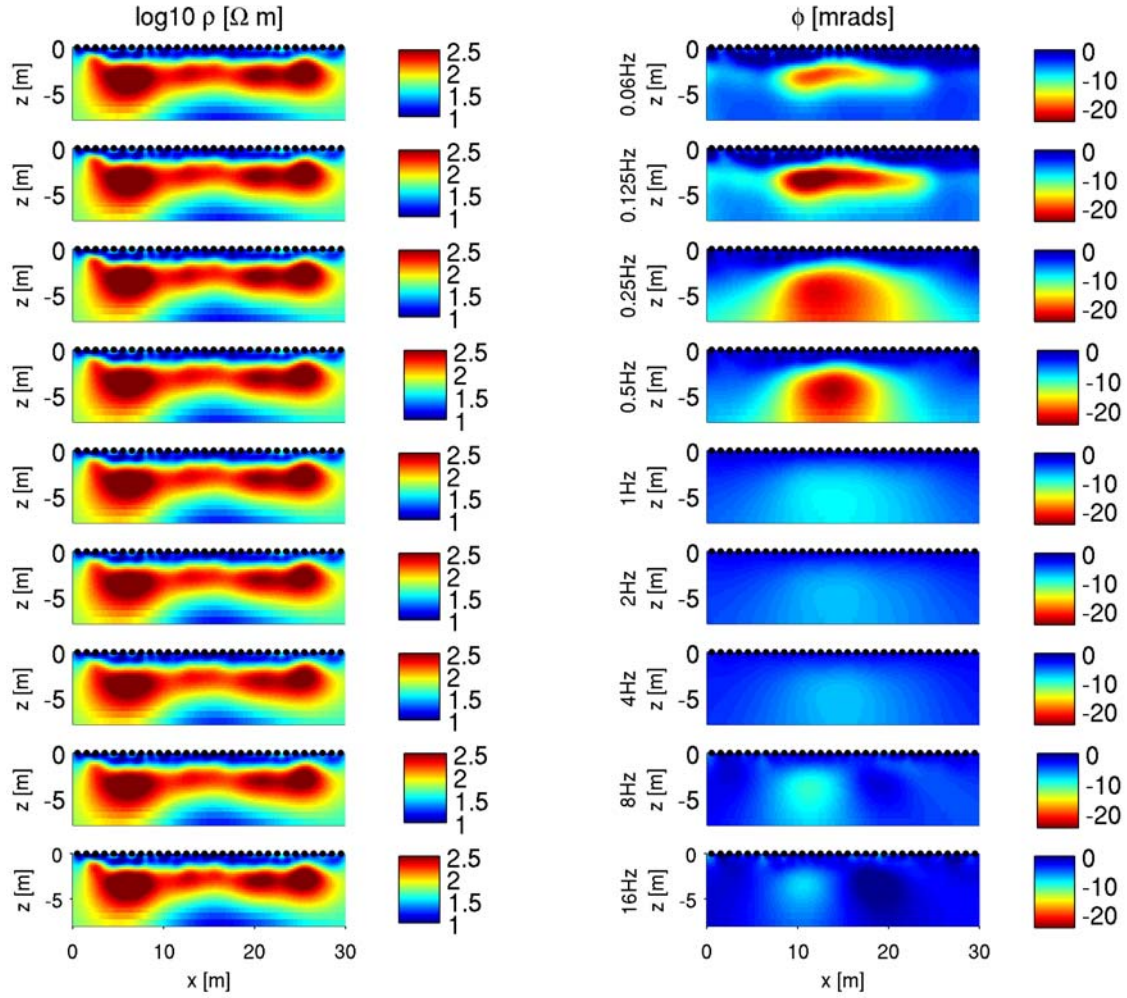


Figure 8: Field SIP imaging results (left: resistivity, right: phase) obtained along a 30 m transect at the US Department of Energy’s Rifle Integrated Field Challenge site near Rifle, Colorado (USA). Reciprocal data were acquired over the 0.06-16 Hz frequency range using a modified dipole-dipole configuration between 30 equally spaced Cu/CuSO₄ electrodes, with a dipole spacing of 4 m and a total of 27 potential dipoles per current dipole.

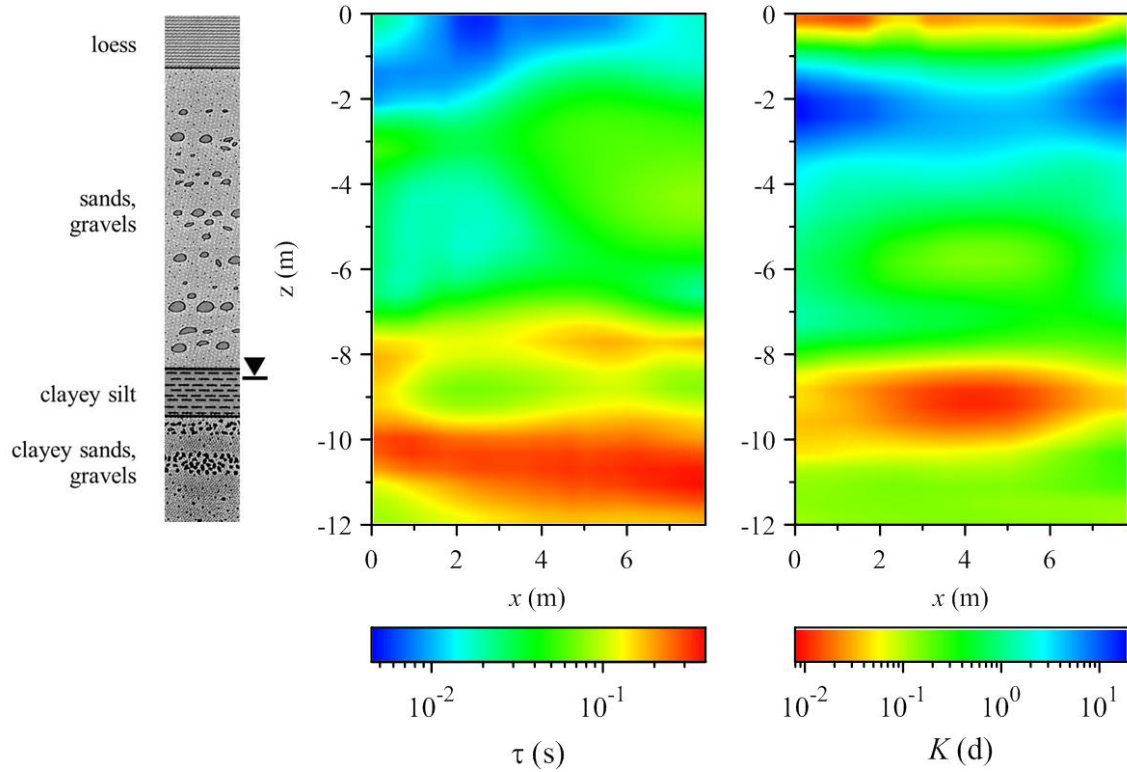


Figure 9: Results from cross-borehole SIP imaging at a site close to the Strasbourg-Entzheim airport (France). Exemplary raw data shown in Figure 6. Left image: IP relaxation time as obtained from post-inversion Cole-Cole model fitting (modified from Kemna et al., 1999). Right image: Hydraulic permeability (in darcies) as estimated from the 0.125 Hz complex resistivity image using the model by Börner et al. (1996) (from Kemna, 2000). Geological log shown for comparison. In the sand-gravel sections, larger relaxation times are observed in the saturated zone than in the vadose zone, indicating larger relaxation lengths in saturated pores. The permeability image in particular delineates the low-permeable clayey silt layer.

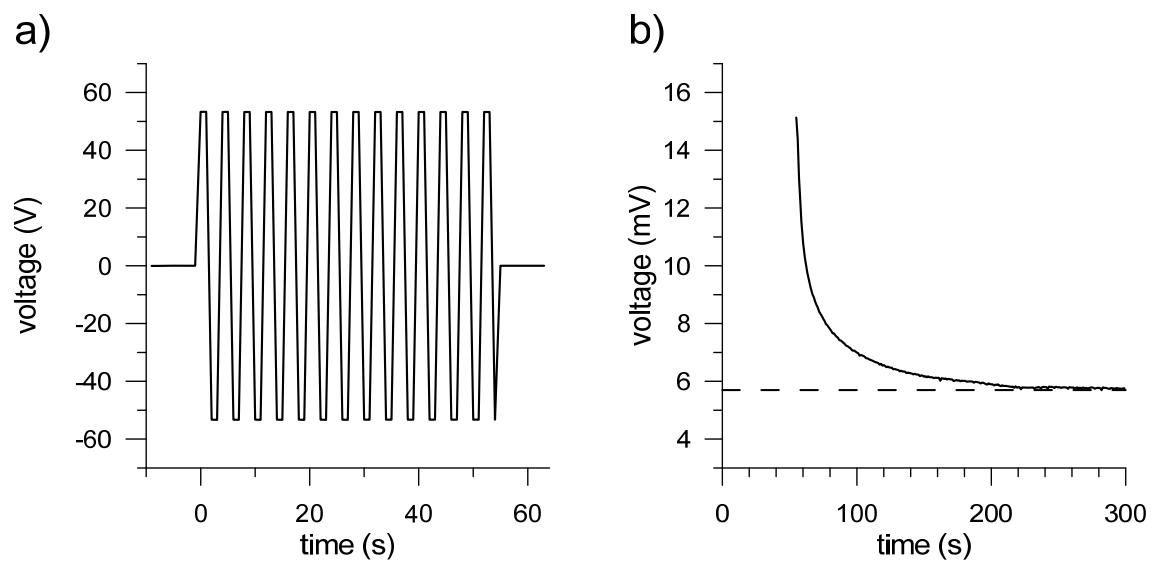


Figure 10: (a) Temporal voltage response of a current transmitting dipole with the following specifications: 4 m dipole spacing; Cu/CuSO₄ electrodes; 55 V transmitting voltage; 0.25 Hz. (b) Voltage decay on the same dipole following cessation of current injection; voltage response due to electrode polarization is below 1 mV (relative to background SP response of ~5.7 mV) after ca. 100 seconds.

DISCLAIMER

This document was prepared as an account of work sponsored by the United States Government. While this document is believed to contain correct information, neither the United States Government nor any agency thereof, nor The Regents of the University of California, nor any of their employees, makes any warranty, express or implied, or assumes any legal responsibility for the accuracy, completeness, or usefulness of any information, apparatus, product, or process disclosed, or represents that its use would not infringe privately owned rights. Reference herein to any specific commercial product, process, or service by its trade name, trademark, manufacturer, or otherwise, does not necessarily constitute or imply its endorsement, recommendation, or favoring by the United States Government or any agency thereof, or The Regents of the University of California. The views and opinions of authors expressed herein do not necessarily state or reflect those of the United States Government or any agency thereof or The Regents of the University of California.

Ernest Orlando Lawrence Berkeley National Laboratory is an equal opportunity employer.